Journal of Biomedical Optics 7(3), 425–434 (July 2002)

Photothermal images of live cells in presence of drug

Dmitri Lapotko
Tat'yana Romanovskaya
International Research Centre
Luikov Heat and Mass Transfer Institute
Minsk, Belarus

Vladimir Zharov
University of Arkansas for Medical Sciences
The Philips Classic Laser Biomedical Laboratory
Little Rock, Arkansas 72205-7199

Abstract. A new method for the study of drug–cell interaction is suggested. It is based on optical monitoring of cell response to drug impact. To detect this response, a high sensitive photothermal imaging technique has been developed. This technique is based on irradiation of the cells with a focused short pulse double-frequency pump laser (532 nm, 8 ns) and monitoring the laser-induced local thermal effects. This is realized with a second collinear dye laser pulse (630 nm, 6 ns) that probes the heated cell absorbing zones. The temperature-dependent variations of the refractive index in the absorbing zones in cross section of probe beam are recorded with phase-contrast technique. The photothermal (PT) image represents a two-dimensional depth-integrated temperature distribution in the irradiated volume and correlates with the conventional optical absorption images. It was experimentally shown that the introduction of NaN_3 or anti-tumor drug in the cell suspension led to a change in the structure of PT images of human lymphocytes and human lympholeukemia cells, respectively. It was hypothesized that the observed effects could be associated with the change of redox state of respiratory chain component. [DOI: 10.1117/1.1481902]

Keywords: drug-cell interaction; light absorption; photothermal imaging; chromophore.

Paper JBO 01037 received May 25, 2001; revised manuscript received Dec. 3, 2001; accepted for publication Jan. 14, 2002.

1 Introduction

Many testing systems have been developed to determine general and specific toxicity at different levels of study: from the gene-expression profile to specific organs, although most of them are relatively expensive and time consuming.[1,2] In comparison with animal and human trials, the study of drug-cell interaction *in vitro* allows us to reduce the sample volume and potential hazard.[3–5] Among various effects used for screening the nonspecific drug action at the cell level, it is worth mentioning in the first place the drug-induced inhibition of protein and DNA synthesis, alteration of transport rates and membrane permeability, impact on energetic processes, and direct destruction effects.[6,7] Worth noting is that drug-induced alteration of the cell metabolism can be monitored through the cell respiration chain (RC) activity[8–10] by means of several methods (polarographic,[11] electrochemical,[12] etc.) including very promising optical microscopy/spectroscopy.

Most spectroscopic assays for the drug action study are based on measuring the absorption of optical radiation by intracellular compounds or endogenous biomolecular markers involved in toxicologic or only inhibitory processes.[13,14] For example, the most universal assay, the transmittance spectroscopy, can be combined with potentiometry to study redox-active hem-proteins.[15] A common problem of transmittance spectroscopy, however, is its relatively low absorption sensitivity, which is due to the small optical path of light in cell microstructures. Therefore, this kind of spectroscopy allows monitoring of only significant drug-induced morphologic cell changes manifested by a long delay after the drug action. Although staining can solve this problem, it has some limitations for the live cell studies. Another potential tool for studying the drug-induced refractive heterogeneous variations in the cell structure is the phase microscopy in different modifications.[16–18] For example, differential-interference contrast microscopy provides information of the drug action through simultaneous monitoring of corresponding changes in the cellular fine structure and organelle motion.[19,20] This method proved to be more sensitive and yielded more specific information on cellular changes than conventional cytotoxicity tests (viability tests with trypan blue staining and lactate dehydrogenase release) performed in parallel. One of the most powerful and sensitive assays, based on fluorescence diagnosis of cytotoxicity, targets only cellular structures that are themselves fluorescent or can be labeled with fluorescent markers.[21–30] Most endogenous biomolecules, however, are nonfluorescent or weakly fluorescent in their native state, while specific fluorescence labeling of targeted structures is difficult, limited by the number of available fluorescent markers, and may lead to unpredictable distortion in cell–drug interactions.[31–38] This state of affairs underscores the need for new assays to overcome the limitations of existing technologies.

One of the alternative approaches can be based on measuring the thermal effects in irradiated samples with photocalorimetric methods [photoacoustic, photothermal (PT), ''thermolens,'' PT radiometry, PT deflection technique, and others].[39–46] These methods with the use of laser sources provide, for nonfluorescent samples, the highest sensitivity for the absorption coefficient, in the order of 10^{-7}–10^{-9} cm^{-1},[41,42] which allows us to evaluate super-

Address all correspondence to Vladimir Zharov. Tel: 501-686-8412; Fax: 501-686-8029; E-mail: zharovvladimirp@uams.edu

small concentrations of molecules with a sensitivity comparable to that of the laser fluorescence methods.[42,44–46] The beam deflection PT calorimetry was successfully used for time-resolved studies of the kinetics of the relaxation processes in molecules in solution.[39,40] Little progress, however, was made in biologic applications of calorimetric methods, especially for studying of live single cells.[46] Besides, there is no information on the application of calorimetric methods for studying the drug action at the cell level.

Recently, a novel dual-laser phase-contrast photothermal imaging (PTI) has been developed.[47–57] PTI is based on irradiating cells with a focused short-pulse pump laser and recording the temperature-dependent variations of the refractive index with phase-contrast imaging of a second collinear laser pulse. It was shown that PT response from different cells is sensitive to different environmental impact including temperature, chemicals, and drugs.[54,55] The objective of this work was further development of the PTI and evaluation of its capability for the study of cell response to drug impact with focus on analyzing the drug-induced alteration of PT image structures.

2 Methods and Materials

2.1 PT-Assay Model

The principle of PT monitoring of drug-induced alterations of intracellular absorbing structures is based on cell irradiation by a pump laser pulse with a wavelength in the spectral range of the potential absorbing biomolecular structures. It is assumed that these structures are sensitive to drug actions and can play the role of natural markers. The absorbed energy, ΔW, in a biomolecular structure with volume V and absorption coefficient α is determined for the case of low absorption, when $\alpha L \ll 1$, in accordance with the following equation:[42]

$$\Delta W \cong dV\Phi\alpha V\Phi, \tag{1}$$

where Φ is laser fluence rate (J/cm^2); L is the target length along the laser beam; $\alpha \cong \sigma N$, where σ is the cross section of absorption, and N the density (concentration) of absorbing biomolecules. A secondary phenomena in the irradiated biomolecules is the relaxation of excitation with transformation of the absorbed energy into heat (nonradiative relaxation), fluorescence (radiative relaxation), or photochemical processes[42] with an appropriate quantum yield η, and characteristic time τ: η_{NR}, τ_{NR}, η_R, τ_R and η_{PH}, τ_{PH}, respectively. The total quantum yield of all three channels of excitation relaxation equals unity, i.e., $\eta_{NR} = 1 - \eta_R - \eta_{PH}$. In pulse laser mode, the local temperature rise in the target can be estimated from the following relatively simple equation:

$$\Delta T \cong \eta_{NR}\Delta W/\rho CV \cong (1 - \eta_R - \eta_{PH})\sigma N\Phi/\rho C, \tag{2}$$

where ρ and C are local density and heat capacity, respectively.

Then, the laser-induced local heating leads to corresponding changes of the temperature-dependent refractive index, n, by the following amount:

$$\Delta n \cong (dn/dT)\Delta T \cong (1 - \eta_R - \eta_{PH})\sigma N\Phi(dn/dT)/\rho C, \tag{3}$$

where dn/dT describes the temperature sensitivity of the refractive index.

In the pulse laser mode, the characteristic heat-dissipation time τ_T, for the local absorbing target is determined by a thermal diffusion process, and that for a target with spherical shape of a radius R ($L = 2R$) is estimated by the following equation:[42,58]

$$\tau_T = R^2/6.75k, \tag{4}$$

where k is thermal diffusivity. For example, for an intracellular target with $R = 35$ nm, an estimation of τ_T is approximately 2 ns (for water parameters). For a cell size of 10 μm, the estimated time τ_T is in the order of 10^{-4} s. When τ_T is measured using Eq. (4), it is possible, when k is known, to obtain information about the value of R.[58] Thus, the size of a submicron particle can be measured by heating the particle with an ultrashort pulse beam ($t_p \ll \tau_T$) of a relatively large diameter that exceeds the wavelength λ, and then by monitoring the cooling process using the PT method. Recently, this approach was successfully demonstrated at two probe delays (10 and 120 ns) with liposomes stained with neutral red absorbing dye as the model of nano-scale absorbing targets.[57] The theoretical limit for this method of determining R is characterized by the time of transformation of absorbed light energy into heat (nonradiative relaxation time τ_{NR}), which is in the order of 10^{-11}–10^{-13} s for condensed matter.[58] According to Eq. (4), this time corresponds to target size of about 1−0,1 nm. Subsequently, in accordance with Eqs. (4) and (3), the PT signal depends on several target parameters including biomolecule concentration, N; cross-section absorption, σ; quantum yield of fluorescence, η_R, and photochemical phenomena, η_{PH} (through the characteristic time τ_{NR}, τ_{PH}, and τ_R); thermodynamic parameters, ρ and C; geometric size, R; and refractive parameters dn/dT. In conventional calorimetric mode, the PT signal amplitude often correlates with the sample absorption coefficient.[42] In our approach, the drug action can be evaluated not only by absorption alteration, but also by changes of other parameters. For example, the drug-induced inhibition of the cell activity can lead to significant changes in biomolecule concentration N,[19] quantum yield,[59] or size of the biomolecular structure R.[19,20] In particular, changes in the redox state of a cell's RC component due to drug impact can lead to altered absorption spectra and quantum yield of photochemical processes.[60] Thus, PT assays can potentially give much more information on drug action than the conventional optical analytic methods.

The limitations of PT absorption sensitivity depend on the background absorption coefficient α_B of the media. In this case, the detection of the local absorbing zone having absorption coefficient α is possible if the local absorption contrast is $\alpha/\alpha_B \geq 1$. It will reach a maximum in the region of minimal absorption by the main component of cells: water, lipids, proteins, and DNA. Water absorbs mainly in the IR region while the other components absorb in the ultraviolet region. Therefore, the optimum spectral region for the most sensitive detection of potential endogenous chromophores ranges approximately between 0.35 and 1 μm, where pure water absorption is about 10^{-3}–10^{-4} cm^{-1} and biological background raises this absorption to at least 10^{-2} cm^{-1}.[42] For example, the potential absorbing chromophores may include

the main RC components such the cytochromes and flavoproteins and other (non-RC) cellular components such as peroxidasa, nonheme Fe–S proteins, cytochrome p450, some porphyrine, etc.[61] For the above mentioned absorption background and $\alpha \sim 10^2 - 10^3$ cm^{-1}, the maximum of absorption contrast will be significant, in the order of $10^4 - 10^5$. In the spectral region where α_B is stronger (UV and IR), up to $10^1 - 10^2$ cm^{-1}, the absorption contrast is much lower, around 10, but nevertheless attainable, up to $\alpha/\alpha_B \sim 2-3$. To detect an object with an absorbtion coefficient of 10^{-2} cm^{-1} and laser-induced temperature of $\Delta T_{\min} = 10^{-2}$ °C, which is two orders higher than what the laser calorimetric methods provide[40–45] and much below the thermal cell damage, in accordance with the theoretical estimation from Eqs. (1)–(4) at $\eta_T \sim 1$, the maximum permissible fluence rate Φ will be about $10^{-2} - 10^{-1}$ J/cm^2. This can be reached by focusing the laser pulse with an energy of $10^{-6} - 10^{-7}$ J onto a 10–20 μm spot. As a result of this analysis, second laser harmonic Nd:yttrium–aluminum–garnet (YAG) with wavelength of 532 nm was chosen to form PT cell images.

Typical sizes of different potential chromophores or their clusters and other absorbing structures may be within a broad range from several nanometers (for example, cytochromes)[62] to hundreds of nanometers and even micrometers (different organelles, mitochondria, etc.). The time-resolved mode with different time delay between pump and probe pulses with time duration around 10 ns allows us, according to Eq. (4), to estimate the average size of absorbing target in the range up to 100 nm. In other words, even if the size of some microzones is smaller than the diffraction spot size, and despite the fact that PT assays allow us to see only diffraction-limited spots on the PT image, an additional measuring of the intensity decrease rate of this spot allows us to estimate the average size of such microzones. Thus, with PTI in time-resolved mode, it is possible to study the absorption of chromophores smaller in size than the laser wavelength, while the PTI, as well as conventional optical microscopes, has spatial resolution limited by the diffraction effects (around 0.8 μm). The thermal diffusion effects lead to the expansion of the initial size of heated zones, so that, some time after the pump laser pulse, the thermal spot will be bigger than the real size of the absorbing zone. When this thermal spot exceeds the diffraction spot diameter, it will be visible in PT images. Of course, temporal resolution is limited and can distort measurements of the smallest targets, because the PT images are recorded with temporal averaging during the probe laser pulse, when some thermal diffusion occurs. However, these distortions will be reduced if targets size is increased.

2.2 Experimental Setup

To measure the pump laser-induced local changes of the refractive index, Δn [Eq. (3)], we used an experimental setup (Figure 1) in phase-contrast mode. In this mode, the parameter Δn is recorded through the change of the phase $\Delta \varphi_{\text{pr}}$ at each point of the cross section (wave front) of the probe beam

$$\Delta \varphi_{\text{pr}} = 2\pi L \Delta n / \lambda. \tag{5}$$

This phase shift is recorded by means of the phase-contrast imaging with the second collinear probe laser pulse. The pump laser-induced variations of the probe-beam phase within

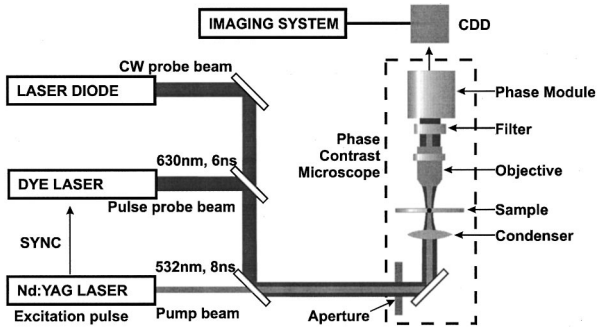

Fig. 1 General setup of the laser photothermal microscope.

the cell are detected by a charge coupled device (CCD) camera (Comfort Inc., St. Petersburg, Russia). In this mode, also referred to as PTI, all data are obtained with one single pump pulse without scanning. The PT image represents a two-dimensional, depth-integrated temperature distribution in the irradiated volume and correlates with the conventional diffraction-limited optical absorption images. The local thermal effects in absorbing microzones are manifested on these images as bright spots on a black background or as three-dimensional (3D) simulations. This mode was used to study PTI microstructures, such as PT signals from local absorbing targets within cells.

In the developed PT microscopic assay (Figure 1), the second harmonic of a Nd:YAG laser (532 nm wavelength) with a pulse energy in the range of 0.1–100 μJ and a 8 ns pulse duration is used as the source of the pump beam. In PTI mode, the source of the probe beam is a pulsed dye laser (630 nm, 6 ns pulse duration). After being mixed with a dichroic mirror, the pump and probe beams are directed coaxially through the aperture and standard microscope condenser into the sample plane. The diameters of pump- and probe-beam spots in this plane are 15 and 12 μm, respectively, and both exceed the diameter of cells ($\sim$10 μm). The pump and probe beams are synchronized, and the time delay between them (fixed at 10 and 120 ns) allows us to study the temporal dynamics of temperature distribution in irradiated cells. After passing through the sample, the pump radiation is cut off with a filter. The phase distribution of the probe beam is converted into amplitude distribution in the conventional phase-contrast microscopic module.

The chosen energy level of the probe laser pulse is 10 nJ, which is much lower (at least one order of magnitude) than the pump-laser energy. This minimizes the influence of possible probe-beam absorption on chromophores at the 630 nm wavelength which can interfere with the thermal effect from the pump laser. Moreover, even if the probe beam were to be absorbed, this effect would not significantly influence the final results because a special algorithm of PT image acquisition had been developed. This algorithm assumes registration of the two probe-beam phase-contrast images: before laser pump pulse $-I^0(x,y,0)$ and after some time-delay τ relative to the pump pulse $-I(x,y,\tau)$. The first image provides information about the initial (background) phase distribution in the cross section of the probe beam itself while the second one brings additional information on the phase change due to absorption pump laser pulse. The difference between them, referred to as

PT image $S(x,y,\tau)$ that can be considered as two-dimensional, depth-integrated temperature distribution in the irradiated cell is determined by the following equation:

$$S(x,y,\tau)\cong[I(x,y,\tau)(E^0{}_{\rm pr}/E^{\tau}{}_{\rm pr})-I^0(x,y,0)]/E_{\rm pm}, \quad (6)$$

where $E^0{}_{\rm pr}$ and $E^{\tau}{}_{\rm pr}$ are probe laser pulse energy values during obtaining images $I^0(x,y,0)$ and $I(x,y,\tau)$, respectively, and $E_{\rm pm}$ is the energy of the pump laser pulse. The ratio $E^0{}_{\rm pr}/E^{\tau}{}_{\rm pr}$ provides necessary compensation of possible variation of probe laser energy from pulse to pulse. Normalization by $E_{\rm pm}$ excludes influence of possible pump pulse energy variations. Thus, the proposed algorithm excludes the influence of laser energy variations on the final results and provides compensation of the phase shift due to possible absorption of the probe beam. Besides, the comparison of PT images at different time delay (τ) gives information on the diffusion effects and cooling time (τ_T) of laser-heated absorbing targets of different size. According to Eq. (4), the cooling time, in its turn, may give information on the average size of the absorbing structures.

Thus, the entire PT-image acquisition procedure includes illumination of the cell with three pulses: probe, pump, and second probe with a delay to pump; then the two probe laser phase-contrast images are recorded, and the differential PT image is calculated according to Eq. (6).

Another feature of PTI in time-resolved mode is the possibility of obtaining separate of PT images with a relatively slow CCD camera response time. In other words the CCD camera allows us to record very short laser pulses, but with some time delay of appearance of PT images. Thus, two of the sequent PT probe images can be obtained with a pump pulse repetition rate no more than 2.5 Hz. On the other hand, the PTI technique allows us to study the dynamic heating–cooling processes with nano-scale time resolution on the basis of time delay variation between pump and probe pulses, but it requires using several laser pump pulses.

The pump and probe beams had a stable Gaussian intensity profile in accuracy range as 2%–3% each. It was experimentally estimated by periodical analyzing of images of both beams with CCD camera without samples. That is why the possible influence of nonsmooth intensity distribution in the cross section (hot point) pump was minimal (practically negligible). On the other hand, the pulse-to-pulse energy variation for pump as well as for probe beam was 5%–10%. To measure laser pulse energy, transparent optical plates were placed on the ways of both laser beams. These plates directed a small part of the laser energy on separate calibrated photodiodes (not shown in Figure 1). An average accuracy of PT image acquisition depended upon many factors (camera error, above-mentioned laser parameter instability, and photodiode error) that were estimated as 4.5%. These factors limited the PTI sensitivity to detect small variations in probe laser images according to the algorithm described in Eq. (6). Laser pulse generation and shutter operations are controlled by software specifically developed for data acquisition and analysis. One computer controls the hardware operation and maintains the desired algorithm, and a second computer handles signal processing.

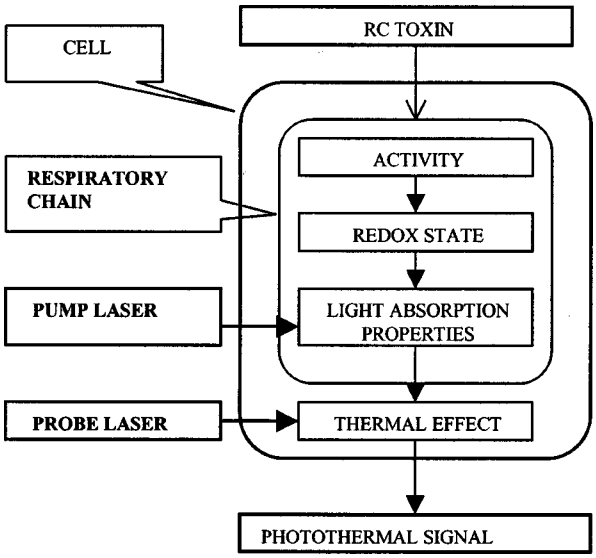

Fig. 2 Schematic diagram for an RC-specific agent-cell interaction model.

Described PT assays have the following advantages: imaging of nonfluorescent structure, which constitutes the majority of native cells; time-resolved imaging, which allows visualization of nano-scale structures; imaging technique that is compatible with a standard biologic microscope, although it does not require a time-consuming scanning mode; high sensitivity (as all photocalorimetric methods) that was several orders of magnitude (at least four) higher absorption sensitivity transmission optical microscopy.[42]

The PT microscope allowed us to also obtain conventional phase-contrast cell images with standard microscope illumination scheme with conventional white light sources as well as with laser illumination with the probe beam. These images referred to below as the optical image are obtained before and after pump pulse within around 1 s and are used for comparison with PT images.

2.3 Experimental Model for Drug–Cell Interaction

For drug–cell interaction models, the key hypothesis was that a drug's nonspecific action leads to changes in cellular light-absorbing ultrastructure that cause corresponding changes in the parameters of PT signals. It is assumed that drug action can be mediated through various biochemical processes and cellular targets of light-absorbing components of the respiratory chain (RC) (Figure 2). Our experimental model assumes comparison of PT signals from single cells between the two cell populations *in vitro*: control with intact cells that include reduced and mainly oxidized forms of the RC components and population of cells with reduced RC components only. The latter is achieved by incubation of cells with sodium aside (NaN_3) which are known as specific inhibitors of RC activity.[63] The NaN_3 blocks the terminal component of the respiratory chain—cytochrome c oxidase—and thus provides the reduction of all RC components in live cells.[64] The first experimental model suggests the modification of the redox state of RC only without the changes in redox state of other cell metalloproteins because NaN_3 does not influence their

redox state. The blood cells (human lymphocytes) that are usually the targets for the drugs chosen for this model.

In the second model we assumed that drugs penetrate into cells, interacting with specific targets in the cells through various potential specific mechanisms. If this interaction, for example, causes toxic effects the cell metabolic rate will change and cell structures may be damaged. For some drugs, such as anti-tumor drugs, interacting with tumor cells, toxic effect is the main drug action. Any suppression of cellular metabolic processes influences RC activity (Figure 2). In general, similar alteration in RC activity may result from different mechanisms of drug action and therefore can be considered as a process that is sensitive to general drug toxic action. The strength of drug effects depends on the drug dose and a cell's functional state (e.g., efflux rate, metabolic rate, etc.). Thus, a drug effect may be different for cells with different rates of differentiation and metabolism. The further processes in the RC that result from drug action will influence the final parameters of PT signal. To study PT images in the presence of a drug in second model we have chosen cells and a drug that is known to inhibit these cells activity. Finally, the dexazone (synthetic hormone that is used as an anti-tumor drug) and chronic lympholeukemia cells (lymphoblasts) with a high level of RC activity have been chosen for this model assuming also the reduction of cell RC components as a result of drug inhibitive action.

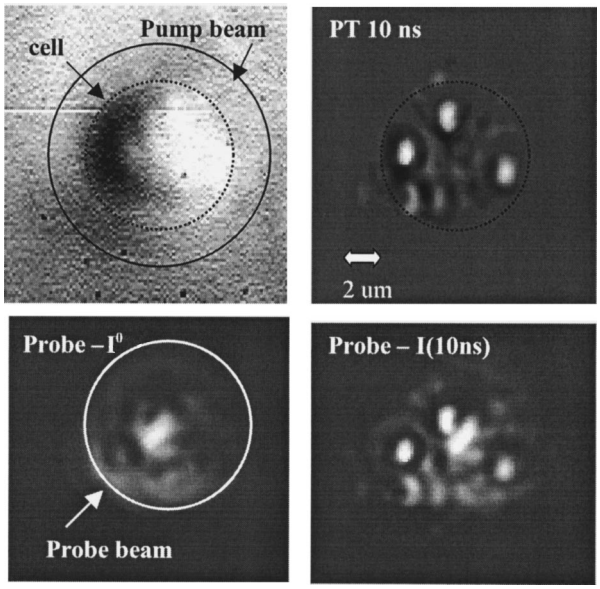

Fig. 3 Images of single human lymphocyte in suspension. Left top: conventional optical phase-contrast image. Right top: PT image as the difference between the probe laser image before (bottom, left) and after pump pulse with 10 ns delay (bottom, right). Pump pulse parameters: 532 nm, 8 ns width, 40 μJ; probe pulse: 630 nm, 6 ns width, 10 nJ.

2.4 Cell Preparation and Handling

As a model of cell–drug interaction human blood lymphocytes and human lympholeukemia cells (L-41) in the presence of NaN_3 solution and anti-tumor drug, respectively, are used *in vitro*. Cell preparation included the following steps: lymphocytes: the population of lymphocytes was separated by centrifuging a leukocytes-containing pellet on Phycoll-Hypaq ($\rho = 1077$ g/cm^2) gradient according to a standard technique.[64] Lymphocytes were treated with 0.85% ammonium chloride solution for 5 min at 37 °C and washed twice with 0.15 M sodium chloride solution containing 0.5% pooled heat-inactivated human AB serum. The suspension was adjusted with the phosphate buffer solution containing 0.5% AB serum to the concentration of 1×10^7 cells per ml and used for analysis. The cell viability was determined by trypan blue dye exclusion and was always higher than 97%. Usually 150 cells have been analyzed from each sample under 20–22 °C. Acquisition time was from 5 to 7 min per sample when optical and PT images were obtained for each cell. Cell lines of chronic lympholeukemia (L-41)—the limphoblasts—were obtained as suspensions from Dialek (Minsk, Belarus). Cell lines were cultivated in standard media and were studied three days after the passage.

Cell images are registered after manual or automatic positioning of the cell with microscope stage with the multisample chamber into the area of the laser beams. The chamber includes a steel case with several glass microcuvettes that can be installed. Each cuvette is $10\times1\times1.5$ mm, with a capillary rectangular channel that is 100×400 μm. Compared with standard microscope slides and coverslips, the cuvette provides a safe and stable environment for living cells and allows monitoring. The ability to study several samples at the same time is very important when one cell population is used as a reference. The amount of suspension required for the cuvette is <1 μl. Each cell for study in the cuvette was chosen according to its conventional optical image. Cell diameters varied in the range 7–10 μm. As the diameter of the Gaussian pump beam at sample plane is 15 μm the decrease of light intensity energy across the cell surface from center to boarders did not exceed 20%–30% and took in account during image acquisition. During the measurements the cells did not change their position at the bottom of the cuvette. Each PT image was obtained with single pump pulse of specified energy. Visual microscopic observation also was used to control cell damage after pump pulse.

3 Results and Discussion

3.1 PT Imaging

The principle of PT imaging is illustrated in Figure 3. Top left shows the conventional phase-contrast optical image of human lymphocyte. This image was obtained at exposure by broadband noncoherent (white) light in the phase-contrast regime of the microscope. This image represents a two-dimensional, depth-integrated refraction distribution in the cell volume. It can be seen that in the case of native cells in suspension such an image does not provide any structural details and they were used in our experiment for cell positioning and for approximate control of cell integrity and size. The bottom left image was obtained with probe laser prior to cell irradiation with pump pulse. This image represents monochrome coherent phase-contrast images of cell optical structure at the moments when the object is not heated. It can be clearly seen that the laser image has more contrast in comparison with the optical image obtained by conventional optical sources. Thus, coherent radiation makes the phase-contrast image more sensitive to refractive index variations. The bot-

tom right image is the same but obtained with 10 ns delay to the pump pulse. Structural changes that are induced by pump pulse absorption and local thermal phenomena can be seen in this image. Subtraction of the first laser image from the second according to Eq. (6) yields the PT image (top right in Figure 3) that gives information only about spatial distribution of intracellular heat distribution and does not depend on possible phase distortion of the probe beam itself. This PT image contains more details in comparison to the optical image (top left in Figure 3). Such a structure may indicate a relatively strong local absorption zone and, respectively, more significant heat release (white spots in Figure 3). Such PT image structures were detected only at 10 ns delay after pump pulse and were not detected at 120 ns delay (not shown). This indicates the local spatial nature of the absorbing structure in these cells. The absence of local details in the PT image at 120 ns means that their cooling time is shorter than 120 ns and therefore the size of the absorbing local zones according to Eq. (4) can be estimated to be at least less than 150 nm. The structure of PT images can be explained by spatially nonuniform distributions of absorbing chromophores in cell. As we have pointed out at 532 nm, there are several absorbing cell components including the RC component flavo proteins and cytochromes and also some metallo proteins outside the respiratory chain including catalase, peroxidase, porphyrins, etc.[63,65] For example, cytochromes that are localized in mitochondria have a characteristic size of 5–7 nm.[62] The peaks at PT image can also be caused by the groups of cytochromes. But the exact identification of the type of absorbing targets needs additional study including obtaining time-resolved PT spectra at different wavelengths of pump laser. Anyway, the visualization of such small structures is not possible with conventional optical microscope diffraction limit that is order 0.6–0.8 μm. Actually the PT image shows thermal ''ghosts'' of small absorbing structures that, due to thermal diffusion, become in time large enough for diffraction-limited optical detection with probe laser.

Another feature of PT images of live lymphocytes is their high heterogeneity in terms of amplitudes and structures among the cells in one population. Optical images of those cells were found to be similar with no such heterogeneity in shape and structure. This result may be explained by the dependence of the RC redox state upon activity of metabolic processes in cells. The degree of such activity may be very different for the lymphocytes within one population.[64] This assumption requires careful verification though when being confirmed experimentally may allow a powerful diagnostic of cell functional state with the PT method.

PT imaging of the cells was performed under the pump pulse energies that cause no damage after cell irradiation with one pump pulse. Noninvasive regime for specific pump energy was verified through the control of cell viability after irradiation of each cell in population with one pump pulse. The cell viability was tested with conventional trepan blue ingestion. The pump pulse was considered to produce no photodamage to cells if the viable cells were no less than 97%, after exposure to pump pulse. Using this criteria we have found that the threshold of photodamage for lymphocytes and lymphoblasts for just one laser pulse was 70 and 55 μJ, respectively. Exposure of one cell to several laser pump pulses caused degradation of PT signals. For example, after 3–10 pulses at energy 20 μJ the amplitude in the peak in some lymphocytes decreased 3–6 times. This phenomena was observed only for the local areas of cells with strong peaks of PT signals. There are at least two explanations for such a response to laser pulse—thermal destruction of absorbing structure or photochemical modification of chromophore molecules with decrease of light absorption or efficacy transformation of absorbed energy into heat. The mechanisms of PT-signal degradation require more study at different pump wavelengths and energy. To avoid the potential influence of such photoinduced modification of cell ultrastructure properties, all further experiments were accomplished with single pump laser pulse exposure, less than mentioned cell photodamage threshold.

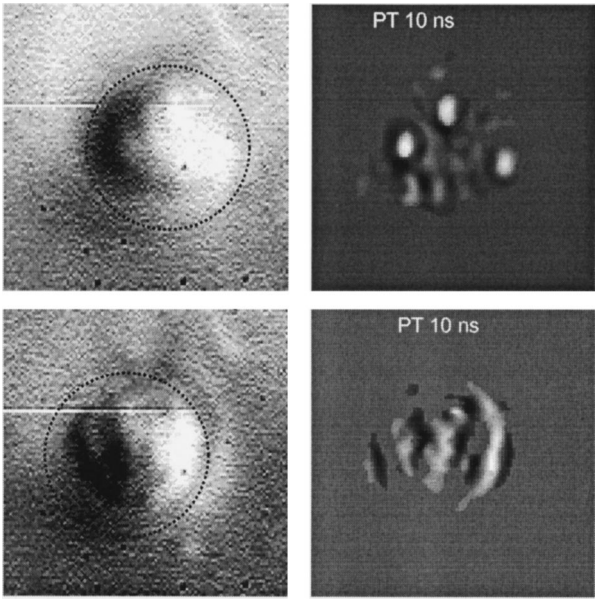

Fig. 4 Influence of NaN_3 on live human lymphocytes *in vitro* in suspension. Conventional optical phase-contrast image (left) and PT images (right) for intact cells (top) and same cells after incubation with NaN_3 (5 mM for 5 min at 37 °C) (bottom). The parameters: pump beam, 532 nm, 8 ns, 40 μJ; probe time delay 10 ns; cell diameter 8 μm.

3.2 Cell PTI Image Alteration in Presence of RC Inhibitor

Prior to the investigation of the drug-cell interaction we have estimated the influence of some inhibiting agent (sodium aside NaN_3) on human lymphocytes *in vitro*. It was assumed that the intracellular target of chemical impact with NaN_3 was of respiratory chain (RC) components.[63] Thus, we expected modeling of alteration in RC through reduction of cell RC components with NaN_3. Two human lymphocyte suspensions were analyzed by acquisition of optical and PT images for 150 cells in each suspension. Pump laser parameters were chosen to obtain the PT image in linear condition without cell photodamage with one pulse at energy 40 μJ (Sec. 3.1). All PT images were obtained at 10 ns delay. It was found (Figure 4) that in comparison with intact cells (right top PT image) incubation of cells for 5 min in 5 mM of sodium azide, a RC inhibitor, resulted in decrease of PT image amplitude (right bottom PT image). Mean PT image amplitude for intact cells

Table 1 PT image parameters of human lymphocytes.

Sample	Mean amplitude, counts	Dispersion, counts	Maximum value, counts
Intact cell	326	442	2024
Test cell (NaN_3) 5 min in 5 mM/ml	153	129	655

was found to be two times higher than for the test cells (Table 1). The most apparent feature of PT images is the disappearance of strong local peaks in PT images of cells. No evident changes were detected for optical phase contrast images between the intact and test cells (Figure 4, top and bottom images, respectively). The observed effects, i.e., the decrease of PT signal at 532 nm, can be explained by the action of NaN_3: this chemical blocks RC cytochrome c-oxidase and reduces the other RC components that absorb at 532 nm—mainly cytochromes. Reduced RC cytochrome forms are known to have slightly higher light-absorption coefficient in comparison to oxidized forms. But the quantum efficiency of photochemical mechanisms of utilization of absorbed energy is significantly higher for reduced forms. This may explain the decrease of heat release in test cells. Although, according to Eqs. (3) and (4), we cannot exclude the influence of other factors that can lead to a change of PT signal parameters including a decrease chromophore absorption or concentration, or changes in their size. The effect of NaN_3 was not the same for all cells and depends upon the degree of activation of metabolic processes in specific cell. Due to this fact experimental data may be obtained with a statistical approach and acquisition of PT images from a sufficient amount of cells. The obtained result was preliminary and lacks the biochemical control of cell populations. But, nevertheless, it demonstrates an ability of PT imaging to monitor RC redox state changes in single live cells. To date, no other method yielded such data.

3.3 Drug–Cell Interaction *in Vitro*

Drug action on cells *in vitro* was studied for the combination of anti-tumor drug (Dexasone) and chronic lympholeukemia cells (lymphoblasts) at cytotoxic doses (Figure 5). Two cell populations were analyzed in the same way as described in Sec. 3.2. PT images of the cells—intact and incubated with the drug (incubation with Dexasone (Dexametasone, KRKA, Slovenia), 0.05 ng/ml/10^6 cells, 5 min at 37 °C)—are shown in Figure 5, right top and bottom PT images, respectively. It can be seen that the influence of the drug provides some changes in PT images. In particular, drug-treated cells do not exhibit strong local PT signals which can be found in PT images of intact cells. One of them is indicated with an arrow in Figure 5, top. In this experiment, as was discussed above, a statistical approach at population level was used. We found that it is more reliable for the detection of the action of a drug because of its different degrees of influence on the different cells. Such heterogeneity may be caused by the nonsynchronized nature of the cell culture that was used. These cells were at different stages of proliferation at the moment of incubation with the drug. Thus the effect of the drug may be a little different for the cells among one population.

Statistical analyses revealed differences for such image parameters as the mean amplitude of PT image and dispersion of the amplitude within the images of intact and treated cells: averaged for the whole population, the amplitude and the dispersion of the amplitude of PT images were 197 and 82 counts, respectively, for intact cells and 149 and 56 counts for drug-treated cells. Student's t test coefficient was $P<0.001$ for mentioned image parameters. These differences in PT signals are expressed much stronger when individual cells are analyzed. In Table 2 the data are given for PT images that are presented in Figure 5. As follows from a comparison of population-averaged and single cell PT image parameters the changes at cell level are stronger that the changes at population level. This result is quite natural and it proves the efficiency of the single cell approach for the detection of drug action on cells. Single cell analysis turns out to be more sensitive due to its ability to register drug-induced changes in cells that may constitute just a small part of number of cells in population. The dose of the drug that was used assumes the following process in these cells—suppression of cell metabolism which should result finally in cell death. This process could be connected with a decreased activity of RC. Therefore results obtained by PT imaging of a cell may be interpreted as the detection of RC redox state change due to drug toxic

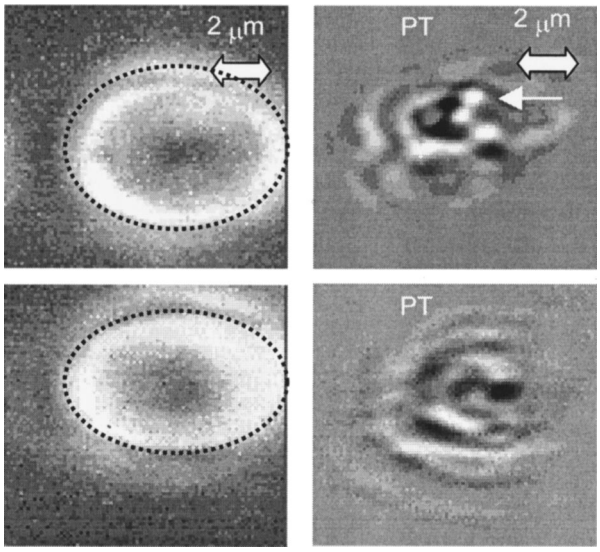

Fig. 5 Influence of an anti-tumor drug on live human lymphoblasts. Optical phase-contrast cell images (left) and PT images (right) for intact cells (top) and after incubation with dexamethasone (0.05 ng/ml/10^6 cells, 5 min at 37 °C) (bottom). Laser pump parameters: 532 nm, 8 ns, 40 μJ; probe: 630 nm, 6 ns, 10 nJ; time delay 10 ns; cell diameter 12 μm. *Arrow* indicates absorption zones.

Table 2 PT image parameters of human lympholeukemia cells (L-41).

Sample	Mean amplitude, counts	Dispersion, counts	Maximum value, counts
Cell population averaged data			
Control	197	82	—
Drug incubated (Dexasone, 0.05 ng/ml/10^6 cells, 5 min at 37 °C)	149	56	—
Single cell data			
Control	450	511	2830
Drug incubated (Dexasone, 0.05 ng/ml/10^6 cells, 5 min at 37 °C)	183	220	811

influence on the cell. The further development of the described approach may allow the control of RC activity in single live cells. Obtained results are rather demonstrative for two reasons: PT studies should be extended into the multiwavelength regime to register PT images at several pump laser wavelengths—for example, 430, 444, 532, and 600 nm with detailed biochemical independent control. Comparison of PT images at different pump laser wavelengths where light absorption coefficient is known to be sensitive to RC redox state (reduced/oxidized) will provide more reliable proofs that specific RC components such as cytochromes to another chromophore are the sources of signal in PT images. In the case of the lymphoblasts the amplitudes in PT images were 1.5–3 times higher than in case lymphocytes (Figure 4) under the same pump energy. This is evident in a stronger absorption on chromophores that could be due to higher rate of ATP synthesis in proliferating cells (blasts) in comparison to mature cells such as blood cells. The higher rate of energetic processes is provided by a larger amount of mitochondria in lymphoblasts and, respectively, higher concentration of chromophores.

4 Conclusions

Our preliminary data demonstrate that PT images of live cells such as lymphocytes and chronic lympholeukemia cells can be obtained without staining with new PT assays. It was also experimentally proved that some parameters of cell PT images, at least structure and amplitude, are sensitive to the action of chemicals and drugs. These results show the principal possibility of application of PT assays for the study of cell–drug interaction at the live single-cell level.

At the current stage, PT image structure should not be associated with the chromophores type and require additional study. The other question that still remains open is the character of the action of different drugs on the same cells and what kind alteration in PT images it produced. The results are qualitative rather than quantitative. Quantitative PT imaging is possible when the correlation between PT image parameters and drug dose will be obtained with independent evaluation of drug action effects with conventional assays. To verify obtained data the PT method may be applied together with the fluorescent method because some endogenous chromophores exhibit natural fluorescence on the one hand and some of the fluorescent probes convert part of the absorbed energy in heat, on the other hand.

Acknowledgments

The authors thank Elena Gordiyko and Natalia Morozova for helpful discussion of the problem and obtained results. This work is supported in part (development of PTI) by the National Science Foundation under grant BES-0119470.

References

1. *Casarett and Doull's Toxicology: The Basic Science of Poisons*, C. D. Klaassen, Ed., 5th ed., McGraw-Hill, New York (1996).
2. S. Farr and R. T. Dunn, ''Concise review: gene expression applied to toxicology,'' *Toxicol. Sci.* **50**(1), 1–9 (1999).
3. C. A. Reinhardt, ''Possibilities of cell culture methods and alternatives to animal tests in toxicology,'' *ALTEX*, **5**(1), 5–14 (1988).
4. M. D. Enger, ''Cellular toxicology,'' *Rev. Environ. Contam Toxicol.* **102**, 79–115 (1988).
5. J. M. Frazier, ''*In vitro* models for toxicological research and testing,'' *Toxicol. Lett.* **68**(1–2), 73–90 (1993).
6. *Molecular Cell Biology*, H. Lodish and D. Baltimore et al., Eds., 3rd ed., p. 654, New York (1995).
7. *Harper's Biochemistry*, R. K. Murrey, D. K. Granner, P. A. Mayes, and V. W. Rodwell, Eds., 21st ed., Appleton & Lange, New York (1988).
8. G. C. Brown, ''Regulation of mitochondrial respiration by nitric oxide inhibition of cytochrome c oxidase,'' *Biochim. Biophys. Acta* **1504**, 46–57 (2001).
9. O. Miro, J. Casademont, A. Barrientos Urbano-Marquez, and F. Cardellach, ''Mitochondrial cytochrome c oxidase inhibition during acute carbon monoxide poisoning,'' *Pharmacol. Toxicol.* **82**, 199–202 (1998).
10. B. Chance and G. R. Williams, ''The respiratory chain and oxidative phosphorylation,'' *Adv. Enzymol.* **17**, 65–69 (1956).
11. T. Kashiwagura, D. Willson, and M. Erecinska, ''Oxygen dependence of cellular metabolism.'' *J. Cell Physiol.* **120**, 13–18 (1984).
12. N. Tokutake, H. Miyoshi, H. Nakazato, and H. Iwamura, ''Inhibition of electron transport of rat-liver mitochondria by synthesized antimycin A analogs,'' *Biochim. Biophys. Acta* **1142**, 262–268 (1993).
13. I. Szundi, G. L. Liao, and O. Einarsdottir, ''Near-infrared time-

resolved optical absorption studies of the reaction of fully reduced cytochrome c oxidase with dioxygen,'' *Biochemistry* **40**, 2332–2339 (2001).
14. C. E. Cooper, M. Cope, R. Springett, P. N. Amess, J. Penrice, L. Tyszczuk, S. Punwani, R. Ordidge, J. Wyatt, and D. T. Delpy, ''Use of mitochondrial inhibitors to demonstrate that cytochrome oxidase near-infrared spectroscopy can measure mitochondrial dysfunction noninvasively in the brain,'' *J. Cereb. Blood Flow Metab.* **19**, 27–38 (1999).
15. P. A. Harmon, R. W. Hendler, W. S. Friauf, and I. W. Levin, ''Combination of potentiometry and spectroscopy for the analysis of a redox protein,'' *Anal. Biochem.* **224**(1), 309–314 (1995).
16. A. Barty, K. A. Nugent, D. Paganin, and A. Roberts, ''Quantitative optical phase microscopy,'' *Opt. Lett.* **23**, 817–819 (1998).
17. E. Cuche, P. Marquet, P. J. Magistretti, and C. Depeursinge, ''Quantitative phase contrast microscopy of living cells by numerical reconstruction of digital holograms,'' *Proc. SPIE* **3604**, 84–89 (1999).
18. M. C. Shin, C. T. Lian, and J. S. Hwang, ''Application of phase contrast microscopy to the study of marine micro-biota,'' *Proc. SPIE* **4082**, 241–245 (2000).
19. D. G. Weiss, ''Videomicroscopic measurements in living cells: dynamic determination of multiple end points for in vitro toxicology,'' *Mol. Toxicol.* **1**, 465–488 (1987).
20. W. Maile, T. Lindl, and D. G. Weiss, ''New methods for cytotoxicity testing: quantitative video microscopy of intracellular motion and mitochondria-specific fluorescence,'' *Mol. Toxicol.* **1**, 427–437 (1987).
21. J. R. Lakowich, *Principles of fluorescence spectroscopy*, Plenum, New York (1993).
22. ''*Cell Biological: Applications of Confocal Microscopy*,'' *Methods in Cell Biology*, B. Matsumoto, Ed., Vol. 38, Academic, New York (1993).
23. K. Konig, ''Multiphoton microscopy in life sciences,'' *J. Microsc.* **200**, 83–104 (2000).
24. W. Denk, J. H. Strickler, and W. W. Webb, ''Two-photon laser scanning fluorescence microscopy,'' *Science* **248**, 73–76 (1990).
25. X. Ronot, L. Benel, M. Adolphe, and J. C. Mounolou, ''Mitochondrial analysis in living cells: the use of rodamine 123 and flow cytometry,'' *Biol. Cell* **57**, 1–7 (1986).
26. H. Schneckenburger, M. H. Gschwend, R. Sailer, W. S. L. Strauss, M. Lyttek, K. Stock, and P. Zipfl, ''Time-resolved *in situ* measurement of mitochondrial malfunction by energy transfer spectroscopy,'' *J. Biomed. Opt.* **5**, 362–366 (2000).
27. M. Poot and R. H. Pierce, ''Detection of changes in mitochondrial function during apoptosis by simultaneous staining with multiple fluorescent dyes and correlated multiparameter flow cytometry,'' *Cytometry* **35**, 311–317 (1999).
28. D. Anderson, T. W. Yu, and M. A. Browne, ''The use of the same image analysis system to detect genetic damage in human lymphocytes treated with doxorubicin in the Comet and fluorescence in situ hybridisation (FISH) assays,'' *Mutat Res.* **390**, 69–77 (1997).
29. N. G. Papadopoulos, G. V. Dedoussis, G. Spanakos, A. D. Gritzapis, C. N. Baxevanis, and M. Papamichail, ''An improved fluorescence assay for the determination of lymphocyte-mediated cytotoxicity using flow cytometry,'' *J. Immunol. Methods* **177**, 101–111 (1994).
30. E. Rocchi, J. Vigo, P. Viallet, I. Bonnard, and J. M. Salmon, ''Multiwavelength videomicrofluorometric study of cytotoxic effects of a marine peptide, didemnin B, on normal and MDR resistant CCRF-CEM cell lines,'' *Anticancer Res.* **20**, 987–996 (2000).
31. M. Muschol, B. R. Dasgupta, and B. M. Salzberg, ''Caffeine interaction with fluorescent calcium indicator dyes,'' *Biophys. J.* **77**(1), 577–586 (1999).
32. V. Jeannot, J. M. Salmon, M. Deumie, and P. Viallet, ''Intracellular accumulation of rhodamine 110 in single living cells,'' *J. Histochem. Cytochem.* **45**(3), 403–412 (1997).
33. D. J. Oh, G. M. Lee, K. Francis, and B. O. Palsson, ''Phototoxicity of the fluorescent membrane dyes PKH2 and PKH26 on the human hematopoietic KG1a progenitor cell line,'' *Cytometry* **36**(4), 312–318 (1999).
34. F. A. Lattanzio, Jr. and D. K. Bartschat, ''The effect of pH on rate constants, ion selectivity and thermodynamic properties of fluorescent calcium and magnesium indicators,'' *Biochem. Biophys. Res. Commun.* **177**(1), 184–191 (1991).
35. A. M. Blackwood, G. A. Sagnella, N. D. Markandu, and G. A. MacGregor, ''Problems associated with using Fura 2 to measure free intracellular calcium concentrations in human red blood cells,'' *J. Hum. Hypertens.* **11**(9), 601–604 (1997).
36. P. L. Johnson, W. Smith, T. C. Baynham, and S. B. Knisley, ''Errors caused by combination of Di-4 ANEPPS and Fluo3/4 for simultaneous measurements of transmembrane potentials and intracellular calcium,'' *Ann. Biomed. Eng.* **27**(4), 563–571 (1999).
37. A. E. Oliver, G. A. Baker, R. D. Fugate, F. Tablin, and J. H. Crowe, ''Effects of temperature on calcium-sensitive fluorescent probes,'' *Biophys. J.* **78**(4), 2116–2126 (2000).
38. ''Application of cellular system in drug metabolism and toxicity studies,'' *Proceeding of a meeting*, Saarland, Germany, July 21–24, 1991, *Toxicology* **82**(1–3), 1–259 (1993).
39. D. E. Falvey, ''Photothermal beam deflection calorimetry in solution photochemistry: recent progress and future prospects,'' *Photochem. Photobiol.* **65**, 4–9 (1997).
40. S. E. Braslavsky and G. E. Heibel, ''Time-resolved photothermal and photoacoustic methods applied to photoinduced processes in solutions,'' *Chem. Rev.* **92**, 1381–1410 (1992).
41. A. C. Tam, ''*Overview of photothermal spectroscopy*,'' in *Photothermal Investigation of Solids and Fluids*, J. Sell, Ed., pp. 1–34, Academic, Boston (1993).
42. V. P. Zharov and V. S. Lethohov, *Laser Optoacoustic Spectroscopy*, Springer Series in Optical Sciences Vol. 37, p. 334, Springer, Berlin (1986).
43. V. P. Zharov, ''*Laser Optoacoustic Spectroscopy in Chromatography*,'' in *Laser Analytical Spectrochemistry*. V. S. Letokhov, Ed., The Adam Hilger Series on Optics and Optoelectronics, pp. 229–271 Hilger, London (1986).
44. M. Tokeshi, M. Uchida, A. Hibara, T. Sawada, and T. Kitamori, ''Determination of subyoctomole amounts of nonfluorescent molecules using a thermal lens microscope: subsingle-molecule determination,'' *Anal. Chem.* **73**, 2112–2116 (2001).
45. H. Kimura, M. Mukaida, T. Kitamori, and T. Sawada, ''Quantitation of drug concentration by thermal lens microscopy in a renal tubule of fixed kidney.'' *Anal. Sci.* **13**, 729–734 (1997).
46. H. Kimura, K. Sekigushi, F. Nagao, M. Mulaida, T. Kitamori, and T. Sawada, ''Imaging of blood antigen distribution on blood cells by thermal lens microscopy,'' *Proc. SPIE* **3916**, 278–284 (2000).
47. D. Lapotko, G. Kuchinsky, H. Antonishina, and H. Scoromnik, ''Laser viability method for red blood cells state monitoring,'' *Proc. SPIE* **2628**, 340–348 (1995).
48. D. Lapotko and G. Kuchinsky, ''Photothermal microscopy for cell imaging and diagnostics,'' *Proc. SPIE* **2390**, 89–100 (1995).
49. D. Lapotko, G. Kuchinsky, M. Potapnev, and D. Pechkovsky, ''Photothermal image cytometry of human neutrophils,'' *Cytometry* **24**, 198–203 (1996).
50. D. O. Lapotko, V. P. Zharov, T. R. Romanovskaya, and G. S. Kuchinskii, ''Investigation of the influence of the photodynamic effect on micro-organisms using the laser photothermal cytometry method,'' *IEEE J. Quantum Electron.* **29**(12), 1060–1065 (1999).
51. D. Lapotko, T. Romanovskaya, G. Kutchinsky, and V. Zharov, ''Photothermal studies of modulating effect of photoactivated chlorin on interaction of blood cells with bacteria,'' *Cytometry* **37**, 320–326 (1999).
52. D. Lapotko, V. Zharov, T. Romanovskaya, and G. Kutchinsky, ''Photothermal microscopy study of photodynamic inactivation of bacteria in the presence of living blood cells,'' *Proc. SPIE* **3592**, 101–109 (1999).
53. D. Lapotoko, T. Romanovskaya, and V. Zharov, ''Photodynamic modulation of immune properties of blood cells,'' *Proc. SPIE* **3914**, 401–410 (2000).
54. D. Lapotko, ''Functional imaging of single cells with photothermal microscopy,'' *Proc. SPIE* **3916**, 268–277 (2000).
55. D. Lapotko and T. Romanovskaya, ''Human cell viability to laser pulse and ion transport processes,'' *Proc. SPIE* **3914**, 262–269 (2000).
56. D. Lapotko and T. Romanovskaya, ''Pharmaceutical applications of photothermal cytometry,'' *Proc. SPIE* **3926**, 228–238 (2000).
57. D. Lapotko, T. Romanovskaya, and V. Zharov, ''Photothermal modification of optical microscope for noninvasive living cell monitoring,'' *Proc. SPIE* **4256**, 43–52 (2001).
58. V. S. Letokhov, ''Effects of transient local heating of spatially and spectrally heterogeneous biotissue by short laser pulses,'' *Nuovo Cimento D* **13**, 939–948 (1991).
59. S. E. Braslavsky, ''Photoacoustic and photothermal methods applied to the study of radiationless deactivation processes in biological sys-

tems and in substances of biological interest,'' *Photochem. Photobiol.* **43**, 667–675 (1986).
60. W. Yahyaoui, J. Harnois, and R. Carpentier, ''Demonstration of thermal dissipation of absorbed quanta during energy-dependent quenching of chlorophyll fluorescence in photosynthetic membranes,'' *FEBS Lett.* **440**, 59–63 (1998).
61. T. Karu, ''Primary and secondary mechanisms of action of visible to near-IR radiation on cells,'' *J. Photochem. Photobiol., B* **49**(1), 1–17 (1999).
62. F. Adar, ''*Electronic absorption spectra of hemes and hemoproteins*,'' in *The Porphyrins*, D. Dolphin, Ed., Vol. 3, pp. 167–182, Academic, New York (1978).
63. T. G. Frey and J. M. Murray, ''Electron microscopy of cytochrome c oxidase crystals. Monomer-dimer relationship and cytochrome c binding site,'' *J. Mol. Biol.* **237**(3), 275–97 (1994).
64. A. L. Lehninger, *Biochemistry: the molecular basis of cell structure and function*, New York, 1972.
65. *Lymphocytes. A practical approach*, G. G. B. Klaus, Ed., p. 30, IRL, Oxford (1987).